

Short Communication

Preparation of Nitrogen Doped Carbon Materials and Analysis of Their Electrochemical Performance

Yue Yuan

School of Optics and Photonics, Beijing Institute of Technology, Beijing, 100081, China
E-mail: yuan Yue000418@163.com

Received: 1 May 2022 / Accepted: 1 June 2022 / Published: 4 July 2022

This paper focused on the preparation and structural and electrochemical characterization of carbon and N-doped carbon as supercapacitive electrode materials. The electrode materials are prepared through crushing, oxidative pretreatment, and bonding, carbonization, and activation, polymer materials processed into carbon-based materials. To make a carbon aerogel electrode material, the N-rich precursors approach was employed to change the obtained carbon substrate material by nitrogen doping. SEM and XRD analyses of morphology and crystal structure revealed that nitrogen was introduced into the doped sample, and that the carbon electrode surface was covered with cloudy clusters and non-uniform aggregated carbon particles, and that the N-doped carbon sample had a spongy structure with interlaced graphite-like thin sheets with higher roughness and porosity, as well as a larger surface. Electrochemical studies of prepared carbon based materials using cyclic voltammetry (CV) and galvanostatic charge discharge (GCD) cycles revealed that N-doped carbon has higher electrochemical capacitive properties than the control sample, as well as desirable fast charge/discharge properties and high power capability for power devices. Specific capacitances of carbon and N-doped carbon were determined to be 13.56 and 192.12 F/g, respectively, at a current density of 1 A/g, implying that specific capacitances of N-doped samples were increased 14 times over undoped material. After 10000 cycles, the cycling stability of N-doped carbon showed almost 108% capacitance retention. The specific capacitance, power, and energy densities of the N-doped carbon supercapacitive electrode were comparable or better than the other reported values of N-doped porous carbon structures, according to a comparison of the N-doped carbon supercapacitive electrode performance with earlier reports regarding porous carbon materials in supercapacitors. These tests showed that the nitrogen doped carbon electrode material generated using the described approach has a lower internal resistance and can retain good electrochemical performance in supercapacitors.

Keywords: Nitrogen doped carbon; Electrochemical performance; Nitrogen-rich precursors; Supercapacitive electrode materials

1. INTRODUCTION

Carbon material is far and away the greatest commercially available electrode material, and it is also one of the hottest research directions in the basic research sector [1, 2]. Carbon has long been a focus of physics, materials science, and electronics researchers due to its unusual structure and excellent physical properties [3-5]. Scientists have been particularly interested in fullerenes, carbon nanotubes, and graphene since their discovery. In certain ways, comprehending carbon is a necessary component for the development of supercapacitors [6, 7]. The primary indicators for evaluating carbon materials as great electrode materials are high specific surface area, acceptable pore structure, surface chemistry, strong conductivity, and high cost performance. The supercapacitor is a novel form of energy storage device with high power density, a long cycle life, and a wide temperature adaption range [8-10]. It has a wide range of applications in a variety of industries, including transportation, energy, and electronic information [11-13].

The composition and structure of supercapacitor electrode materials have an impact on the overall performance and application domains of supercapacitors [14, 15]. According to research, carbon materials' distinctive physical and chemical properties are determined not only by their developed specific surface area, but also by the type, number, and bonding mode of doped atoms on the surface [16, 17]. Nitrogen is a significant component of carbon materials' surface modification. Furthermore, the inclusion of nitrogen-containing functional groups can increase the electron donor's properties on the material's surface, as well as the specific capacitance and power performance of carbon materials [18, 19]. The study of the surface properties of carbon materials has become increasingly popular in recent years. One of the most important variables determining the electrochemical performance of capacitors is surface functional groups. The characteristics of materials can be effectively improved by inserting some heteroatom functional groups [20, 21]. After years of investigation, researchers have discovered that the doped changed atoms include mostly nitrogen, phosphorus, boron, halogen, and other elements. When utilized in supercapacitors, doping the carbon material with heteroatoms can significantly improve its electrochemical performance [22, 23]. The enhancement of electrochemical performance can be shown in two ways: first, the capacitance provided by the heteroatom functional group can raise the capacitor's capacitance ratio; and second, the heteroatom functional group can improve the carbon material's surface wettability. This optimizes the usage of specific surface areas and facilitates the passage of electrolyte ions in the interior pores [24, 25].

Because nitrogen is close to carbon in the periodic table of elements and has a similar atomic diameter to carbon, nitrogen doping is the most commonly investigated modification approach at the moment [26, 27]. As a result, the material structure will not change appreciably as carbon is replaced by the atmosphere. Simultaneously, nitrogen atom doping can effectively change the shape, structure, and chemical properties of carbon materials, improving their qualities in practical applications [28-30]. Carbon post-treatment and carbonization-activated nitrogen-rich precursors are the two most common processes for creating nitrogen doped carbon materials, both of which have varying effects on the final material's performance [31, 32]. The standard electrode material production procedure is time-

consuming, and a certain number of hazardous compounds are produced in the process [33]. The cost of preparing the electrode material will be affected by the processing of these by-products.

Polymer plastics, polymer resins, and several natural polymer compounds are now employed as polymer material precursors. Polymer materials not only have a lot of sources but also have a controlled structure, which has gotten a lot of attention. As high molecular polymers, plastics include polyvinyl chloride, polypropylene, polytetrachloroethylene, polyurethane, polyethylene terephthalate, and others [34]. These polymer raw materials come from a variety of places, allowing them to efficiently eliminate carbon material preparation loss. When heteroatoms are introduced into the carbon framework, various defects with unpaired electrons, such as dislocation, bending, and dislocation, develop in the plane layer of graphite microcrystalline [35]. Heteroatoms can create local surface functional groups at the same time, giving carbon materials' surfaces an acid-base characteristic. According to the diverse combinations of nitrogen atoms and carbon atoms, nitrogen atoms in carbon materials can be classified into chemical nitrogen and structural nitrogen, as indicated in the diagram below. Chemical nitrogen is mostly found on the material's surface in the form of surface functional groups that supply alkali sites for the material, such as the oxygen group and other helium-containing surface functional groups [36]. This type of nitrogen-containing functional group has a high alkalinity and is easy to react with, but it has low stability, is easily decomposed at high temperatures, and falls off easily. Structural nitrogen is nitrogen bound to the skeleton and carbon atoms of a carbon substance to increase the material's L-alkalinity [37, 38].

A range of nitrogen-doped carbon materials with innovative structures and distinctive performance have been produced in recent years as a result of the development of N-doped carbon materials [39]. N-doped carbon materials are now prepared in two ways: nitrogen rich precursors carbonization (in-situ nitrogen doping) and nitrogen-containing functional groups added into porous carbon materials after treatment. N-doped carbon aerogels were made using nitrogen-rich precursors in this study. During the manufacture of the materials, nitrogen atoms were directly incorporated into the carbon skeleton, ensuring that the nitrogen components in the final materials were equally distributed and mostly existed in the form of structural nitrogen [40]

The preparation and electrochemical performance of carbon and nitrogen doped carbon as supercapacitive electrode materials were examined and analyzed based on the aforesaid study. In this study, organic aerogels were successfully made using resorcinol and formaldehyde (RF) as precursors and sodium carbonate as a catalyst. Carbon aerogels are created by carbonizing at a high temperature. According to the order of experimental operation, the preparation of carbon aerogels can be split into six steps: solution preparation, sol-gel reaction, pickling aging, solvent exchange, drying process, and high temperature carbonization. The structural change of resorcinol formaldehyde carbon aerogel during preparation is depicted in the diagram below.

2. EXPERIMENTS

2.1. Preparation of carbon electrode

In this work, polymer materials were employed to prepare carbon materials using the following procedure: The mixture of 5g aniline (99.5%, Sigma-Aldrich) and 4g styrene (99.9%, Sigma-Aldrich)

as carbon sources was oxidized with 5ml of liquid oxidant H₂SO₄ (98%, Sigma-Aldrich). The oxidation treatment reduced the activation temperature, shortened the activation time, and improved the material's surface activity, all of which helped to improve the porosity and carbon yield. After the binder had bound and created the strong oxidized material powder, it was dried at 450°C and carbonized [41]. Place the dried material in an electric constant temperature drying oven and gradually raise the temperature to 160 °C for about 15 minutes. The temperature was then increased to 280°C, completing the initial carbonization process. The temperature was maintained between 280 and 400 degrees Celsius, and the substance altered chemically. After carbonization, 0.5g KOH (99%, Sigma-Aldrich), 0.5g ZnO (99.99%, Sigma-Aldrich) and 0.5ml HCl (37%, Sigma-Aldrich) were used to activate the carbonized material, and the blocked holes in the material were opened or further expanded. The material was deposited after activation, and the preparation of carbon-based compounds was accomplished. The carbon structure was produced and dispersed in an ethanol solution before being cast on a glassy carbon electrode (GCE) to serve as a working electrode.

2.2. Preparation of nitrogen doped carbon electrode

In a 1:2 ratio, 5g of resorcinol (98.5%, Sigma-Aldrich) was dissolved in a tiny amount of deionized water, and formaldehyde (37%, Sigma-Aldrich) was added to make a nitrogen doped carbon electrode. Then, as a catalyst, 0.5 grams of sodium carbonate (99.5%, Sigma-Aldrich) solution was added to the combined solution, adjusted to a certain concentration, and the solutes in the solution were uniformly mixed under magnetic stirring. The mixture was then transferred to a sealed container. The density of the RF aerogel was determined by the ratio of resorcinol, formaldehyde, and water used in this method. The faster the reaction solution gels and the stronger the structural strength of the resulting aerogel, the higher the theoretical density delivered [42]. After configuring the solution, it was transferred into a sealed container and cleaned for 5 minutes in an ultrasonic cleaner before being placed in a constant temperature water bath at 600°C for the sol-gel reaction. The RF solution steadily solidified as the reaction progressed, and the color deepened. The hydrogel was generated and taken from the sealed container after 120 minutes. The product was steeped in a mixture of acetone (99.5%, Sigma-Aldrich) and trifluoroacetic acid (99.0%, Sigma-Aldrich) in a volume ratio of 97:3 for around 3 days for the pickling and aging process. The color of the gel deepened after pickling and aging. To reduce the amount of water in the gel, the original immersion liquid was drained out and the gel was soaked in an acetone solution for 15 minutes before being refilled with additional acetone. Following that, supercritical drying was carried out as follows: The RF aerogels were placed in the temperature-controlled tube furnace's quartz tube in the middle. To drain the moisture absorbed by the organic aerogel samples, the temperature of the zone was stabilized, vacuumed, and heated to 150°C for 2 hours. The quartz tube was filled with inert Ar gas until it reached the same pressure as the outside. The inert gas flow was managed through the exhaust valve, and it was gradually heated to 1050°C at a set pace and remained steady for 15 minutes. After cooling to room temperature, RF carbon aerogels were produced. The preparation of nitrogen doped carbon electrode material was finally finished [43].

2.3. Structural and electrochemical characterizations

Using a Rigaku RINT-2100 X-ray diffractometer (XRD) system with Cu K radiation ($\lambda = 1.5406$), the crystal line phases of the produced carbon-based materials were studied. A scanning electron microscope was used to examine the morphology (SEM; Zeiss 510 META confocal microscope, Carl Zeiss, Germany). The CHI 660C electrochemical workstation with a three-electrode configuration was used to study the electrochemical properties of prepared carbon-based materials using cyclic voltammetry (CV) and galvanostatic charge discharge (GCD) cycles. The modified GCE with carbon and N-doped carbon as working electrode, Pt plate as a counter, and Ag/AgCl as a reference electrode was used. As the electrolyte, a 1 M H₂SO₄ aqueous solution was utilized.

3. RESULTS AND DISCUSSION

3.1. Analyses of morphology and crystal structure

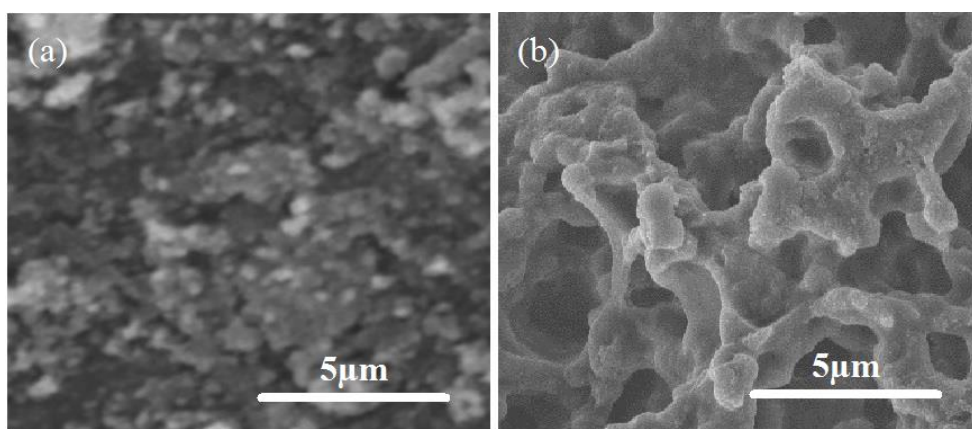


Figure 1. SEM images of (a) carbon and (b) N-doped carbon.

Figure 1 shows SEM images of carbon and N-doped carbon. The surface of the carbon electrode in Figure 1a is covered with hazy clusters, and non-uniform aggregated carbon particles with an average diameter of 0.5 μm are visible. In Figure 1b, SEM images of N-doped carbon show that the doped sample has a spongy structure, containing interlaced graphite-like thin sheets with a large surface and wrinkled edge, which can not only suppress aggregation of N-doped carbon layers but also increase roughness and porosity, improving the catalytic activity and surface area of the doped carbon electrode.

Figure 2 shows XRD readings of carbon and N-doped carbon. Both samples have two distinct XRD peaks at $2\theta=25.39^\circ$ and 43.98° , respectively, corresponding to the (002) and (100) planes of hexagonal graphite structures [44], respectively. The crystalline area of the N-doped carbon electrode

can be attributed to the relatively faint diffraction peaks at $2\theta = 33.27^\circ$ in the XRD pattern of N-doped carbon [45, 46].

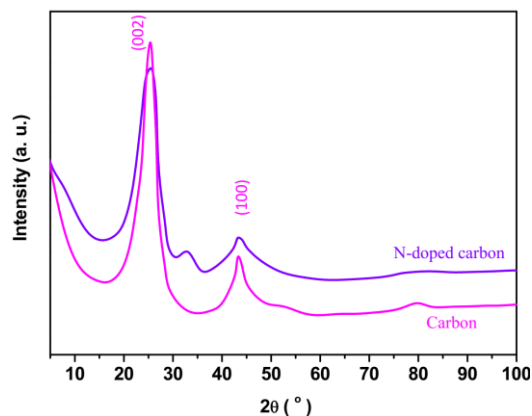


Figure 2. XRD measurements carbon and N-doped carbon.

3.2. Electrochemical analyses

CV and galvanostatic charge/discharge analyses were used to assess the electrochemical activity of carbon and N-doped carbon. Figure 3 shows CV curves of samples in 1M H₂SO₄ solution as the electrolyte solution at a scan rate of 10mV/s. The quinone/hydroquinone reaction of surface oxygenated groups on the carbon structure is linked to the redox peak in the CV curve of an undoped carbon sample, as displayed [47, 48].

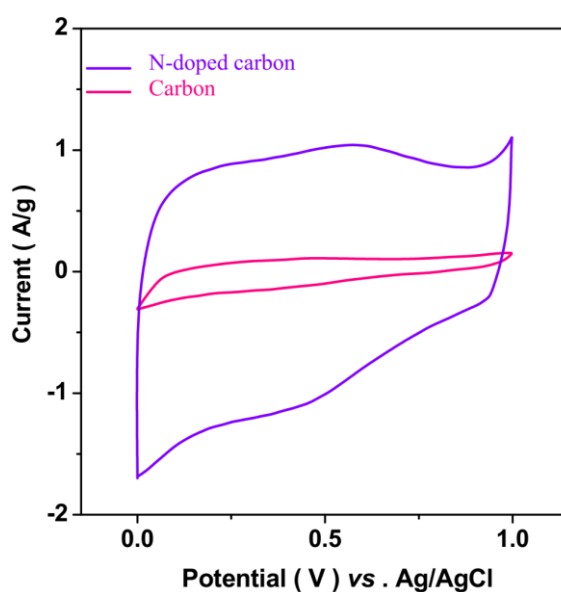


Figure 3. The CV curves of carbon and N-doped carbon at a scan rate of 10 mV/s in 1M H₂SO₄ solution as the electrolyte solution.

Both carbon and N-doped carbon CV curves are comparable, and the development of humps in the CV curves indicates redox processes linked with heteroatom functionalities of the materials [49], especially heteroatom N, which is introduced in the carbon structure [50]. The redox peak in the CV curve becomes less apparent after doping, while a redox hump appears at a higher potential. Furthermore, N-doped carbon has a bigger area under the CV curve, indicating that it has a stronger electrochemical capacitive property than the unhopeful sample [51], which can be related to a larger effective surface area [52]. Moreover, it is suggested that the nitrogen functional groups have an effect on pseudocapacitance, and show an enhancing effect on energy storage performance because of the presence of a positive charge [53, 54]. Therefore, N-doping can improve electron transfer at high current loads [53].

The observed CV curves for carbon and N-doped carbon at various scan speeds are shown in Figures 4a and 4b, respectively. When the scan rate was steadily increased from 10 to 100 mV/s, the current increased as well. With increased scan rate, the morphologies of N-doped carbon are slightly modified, and a regular rectangular shape is obtained without visible redox, demonstrating outstanding capacitance performance at a high scan rate and an optimal capacitive property [55, 56]. The little tilted rectangular-like shape is observed for the CV curve at a scan rate of 200 mV/s, indicating the desirable fast charge/discharge property and high power capability for power devices [57, 58].

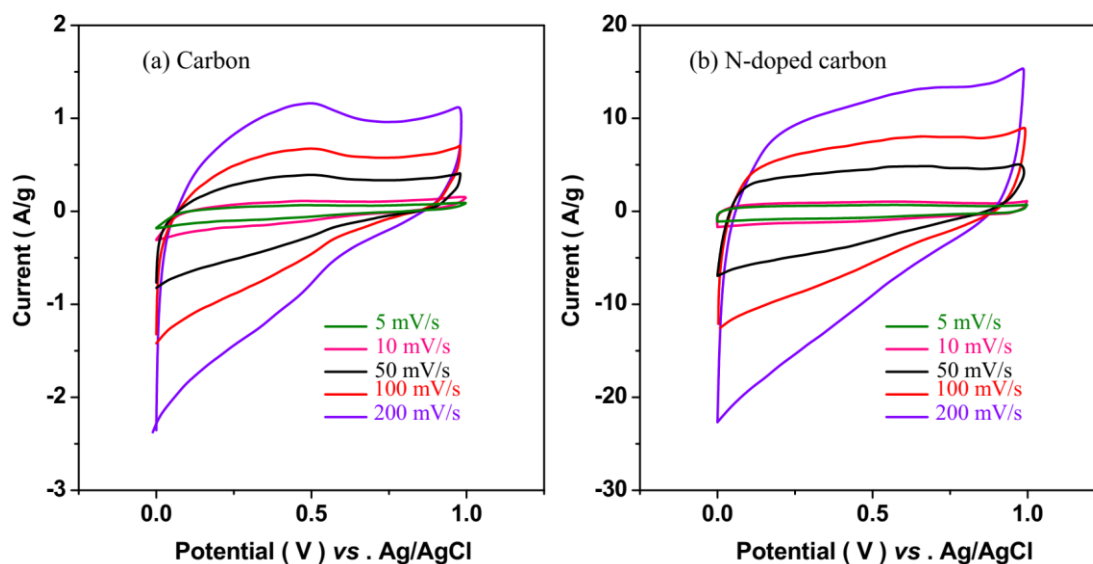


Figure 4. The obtained CV curves for (a) carbon and (b) N-doped carbon at various scan rates in 1M H_2SO_4 solution as the electrolyte solution.

GCD tests are assumed to be the most accurate technique for supercapacitors [55, 57]. As shown in Figure 5a, the electrochemical characteristics, capacitance, and rate capability of carbon and N-doped carbon were also investigated using GCD at 1 A/g. The GCD curves show that the N-doped carbon electrode has the fastest charging and discharging periods, meaning the largest specific

capacitance, which is consistent with CV results in Figure 4. The specific capacitances (C_s) of both samples can be determined from the GCD curve according to the following equation [59, 60]:

$$C_s = \frac{I\Delta t}{m\Delta V} \quad (1)$$

Where I and Δt are the discharge current and the discharge time, respectively. m is the mass of active materials on the electrode, and ΔV is the voltage change during the discharge process. C_s values of carbon and the N-doped carbon are determined to be 13.56 and 192.12 F/g, respectively, indicating the C_s of the N-doped sample is enhanced by ~ 14 times compared to the undoped sample. This significant increase in C_s value can be attributed to an increase in pseudocapacitance caused by nitrogen functionalities groups located around the carbon [59, 61]. First, it is found that the ohmic voltage drop in the discharge curve is correlated with the resistance of the electrode. The voltage drops for carbon and N-doped carbon are 0.149 and 0.011 V, respectively, at 1 A/g. Thus, N doping decreases the electrode resistance [62, 63]. It has been reported that nitrogen doping can effectively enhance the wettability of carbon with electrolyte, and increase the electrical conductivity and capacitive properties [64]. Figure 5b shows the GCD curves of N-doped carbon with various current densities from 0.1 to 1 A/g which reveal good symmetry and fairly linear slopes for recorded GCD curves, illustrating the smooth charge or discharge behavior, fast Faraday redox reaction, and better capacitive behavior [59, 61, 65, 66].

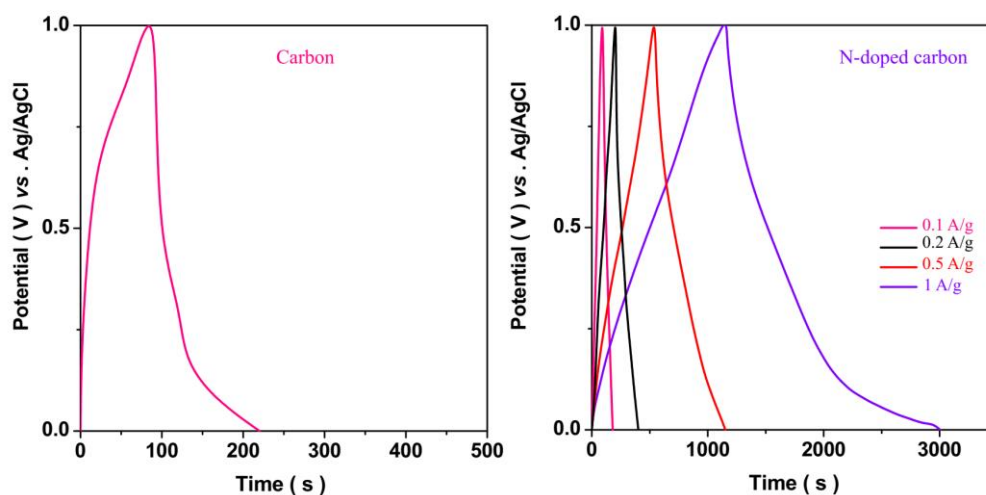


Figure 5. (a) Galvanostatic charge/discharge (GCD) curves of carbon at 1 A/g; (b) GCD curves of N-doped carbon with various current densities from 0.1 to 1 A/g in the potential window of 0 to 1 V at a scan rate of 10 mV/s in a 1 M H₂SO₄ aqueous solution.

In supercapacitor applications, long-term cycle stability is a critical parameter. GCD cycling was used to test the cycling stability of N-doped carbon at current densities of 1 A/g during 10000 continuous cycles in the potential window of 0 to 1 V in a 1 M H₂SO₄ aqueous solution. At a current density of 1 A/g, Figure 6 displays the capacitance of N-doped carbon in terms of cycle number. Figure 6 shows that after 10000 cycles, over 108 percent of the capacitance is retained, proving the high cycling durability of N-doped carbon as a supercapacitive electrode material due to the N-doped

carbon's superior physical stability [64, 67, 68]. The N-doped carbon electrode has a spongy structure of interlaced graphite-like thin sheets, as well as a large surface and wrinkled edge, which provides a rough and porous surface that facilitates charge transport properties and may lead to efficient capacitance retention [62, 64], which is in good agreement with the results of SEM in Figure 1.

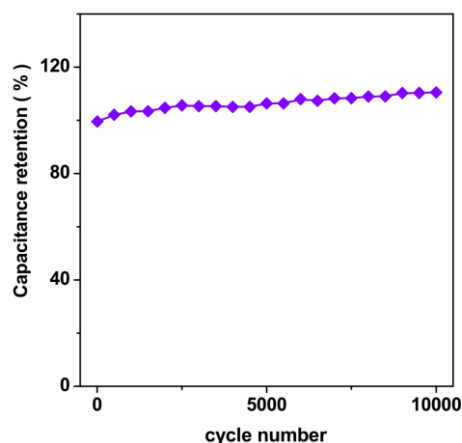


Figure 6. Capacitance retention of the N-doped carbon in term of cycle number at a current density of 1 A/g over 10000 continuous cycles in the potential window of 0 to 1 V in a 1 M H₂SO₄ aqueous solution.

3.3. Comparison the supercapacitive electrode performance

The specific capacitance of the N-doped carbon is comparable to the reported values of N-doped porous carbon nanofibers [69, 70], enriched N-doped graphene [71], and N-doped mesoporous carbons [72]. The specific energy (E) and power density (P) of supercapacitor cells can be calculated by the following equations [73, 74]:

$$E = \frac{1000 \times \frac{1}{2} C_s (\Delta V)^2}{3600} \quad (2)$$

$$P = \frac{E}{\Delta t} \times 1000 \quad (3)$$

Figure 7 shows energy density vs. power density and illustrates the relationship between energy density and power density obtained for different charge–discharge current densities (0.1, 0.2, 0.5, 1 A/g). As seen, the power and energy densities for N-doped carbon as the supercapacitive electrode are comparable or better than reported values for earlier reports regarding porous carbon materials in supercapacitors such as hierarchically porous carbon [75], cross-linked carbon nanofiber [76], Br and N co-doped porous carbon [77], N and B co-doped KOH-activated bamboo-derived carbon [78] and porous carbon nanofiber [79, 80].

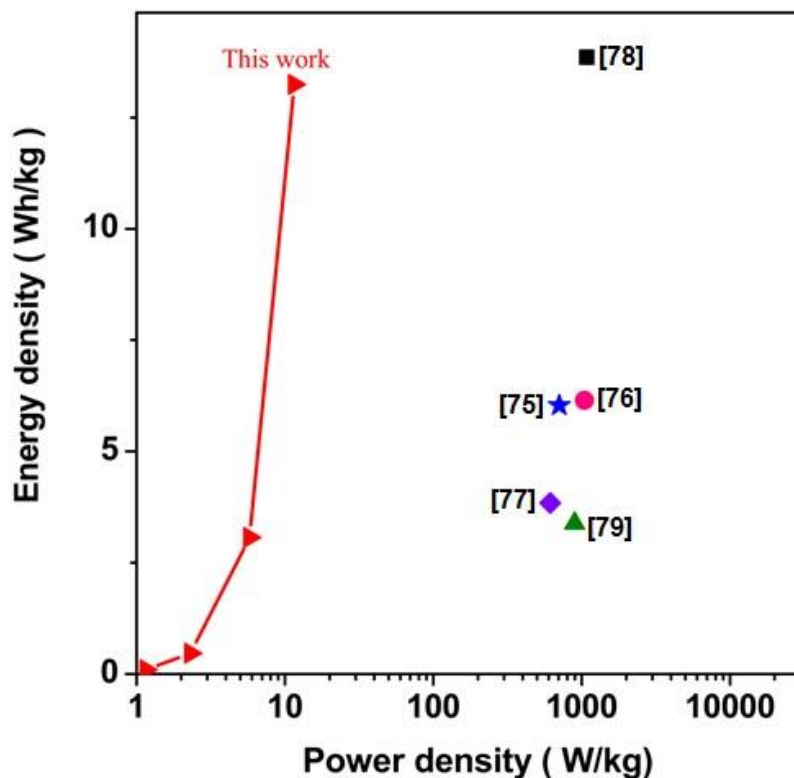


Figure 7. Energy density vs. power density for this work and earlier reports of supercapacitors such as hierarchically porous carbon [75], cross-linked carbon nanofiber [76], Br and N co-doped porous carbon [77], N and B co-doped KOH-activated bamboo-derived carbon [78] and porous carbon nanofiber [79].

4. CONCLUSION

In summary, the synthesis and structural and electrochemical characterization of carbon and N-doped carbon as supercapacitive electrode materials were the focus of this research. Crushing, oxidative pretreatment, and bonding, carbonization, and activation, polymer materials converted into carbon-based materials are used to make electrode materials. To make a carbon aerogel electrode material, the N-rich precursors approach was employed to change the obtained carbon substrate material by nitrogen doping. Analyses of morphology and crystal structure revealed that nitrogen was introduced into the doped sample, and that the carbon electrode surface was covered with cloudy clusters and non-uniform aggregated carbon particles, and that the N-doped carbon sample had a spongy structure with interlaced graphite-like thin sheets with higher roughness and porosity, as well as a larger surface and wrinkled edge. Electrochemical tests of produced carbon based materials revealed that N-doped carbon had stronger electrochemical capacitance properties than the control sample, as well as desirable fast charge/discharge properties and high power capability for power devices. At current density of 1 A/g, specific capacitances of carbon and N-doped carbon were determined to be 13.56 and 192.12 F/g, respectively, suggesting that specific capacitances of N-doped samples were increased by 14 times compared to undoped material. Furthermore, GCD investigations of N-doped carbon with varied current densities indicated smooth charge or discharge behavior, a quick Faraday redox reaction, and

improved capacitance. The cycling stability of N-doped carbon was studied and found to be almost 108% capacitance retention after 10000 cycles, suggesting that N-doped carbon as a supercapacitive electrode carbon has excellent cycling stability due to its superior physical stabilities. The specific capacitance, power, and energy densities of the N-doped carbon supercapacitive electrode were comparable or better than the other reported values of N-doped porous carbon structures, according to a comparison of the N-doped carbon supercapacitive electrode performance with earlier reports regarding porous carbon materials in supercapacitors. These tests showed that the nitrogen doped carbon electrode material generated using the described approach has a lower internal resistance and can retain good electrochemical performance in supercapacitors.

References

1. K. Kumarasinghe, G. Kumara, R. Rajapakse, D. Liyanage and K. Tennakone, *Organic electronics*, 71 (2019) 93.
2. Q.-M. Xiong, Z. Chen, J.-T. Huang, M. Zhang, H. Song, X.-F. Hou, X.-B. Li and Z.-J. Feng, *Rare Metals*, 39 (2020) 589.
3. X. Chen, J.A. Rogers, S.P. Lacour, W. Hu and D.-H. Kim, *Chemical Society Reviews*, 48 (2019) 1431.
4. X. Zhang, Y. Tang, F. Zhang and C.S. Lee, *Advanced energy materials*, 6 (2016) 1502588.
5. D. Jia, Y. Zhang, C. Li, M. Yang, T. Gao, Z. Said and S. Sharma, *Tribology International*, 169 (2022) 107461.
6. Y. Gong, R. Chen, H. Xu, C. Yu, X. Zhao, Y. Sun, Z. Hui, J. Zhou, J. An and Z. Du, *Nanoscale*, 11 (2019) 2492.
7. B. Ji, F. Zhang, X. Song and Y. Tang, *Advanced materials*, 29 (2017) 1700519.
8. H. Wang, M. Wang and Y. Tang, *Energy Storage Materials*, 13 (2018) 1.
9. M. Wang, C. Jiang, S. Zhang, X. Song, Y. Tang and H.-M. Cheng, *Nature chemistry*, 10 (2018) 667.
10. H. Li, Y. Zhang, C. Li, Z. Zhou, X. Nie, Y. Chen, H. Cao, B. Liu, N. Zhang and Z. Said, *Korean Journal of Chemical Engineering*, 39 (2022) 1107.
11. S. He, S. Wang, H. Chen, X. Hou and Z. Shao, *Journal of Materials Chemistry A*, 8 (2020) 2571.
12. D. Gong, C. Wei, D. Xie and Y. Tang, *Chemical Engineering Journal*, 431 (2022) 133444.
13. C. Liu and J. Rouhi, *RSC Advances*, 11 (2021) 9933.
14. S. Dou, P. Li, D. Tan, H. Li, L. Ren and F. Wei, *Energy*, 227 (2021) 120540.
15. B. Ji, J. Gou, Y. Zheng, X. Zhou, P. Kidkhunthod, Y. Wang, Q. Tang and Y. Tang, *Advanced Materials*, (2022) 2202714.
16. Y. Zhou, Z. Sun, L. Jiang, S. Chen, J. Ma and F. Zhou, *Applied Surface Science*, 533 (2020) 147431.
17. B. Li, C. Li, Y. Zhang, Y. Wang, D. Jia and M. Yang, *Chinese Journal of Aeronautics*, 29 (2016) 1084.
18. H. Zhang, B. Zhang, C. Di, M.C. Ali, J. Chen, Z. Li, J. Si, H. Zhang and H. Qiu, *Nanoscale*, 10 (2018) 5342.
19. J. Zhou, J. Bai and Y. Liu, *Micromachines*, 13 (2022) 781.
20. F. Koyuncu, F. Güzel and İ.I.G. İnal, *Diamond and Related Materials*, 124 (2022) 108920.
21. T. Li, D. Shang, S. Gao, B. Wang, H. Kong, G. Yang, W. Shu, P. Xu and G. Wei, *Biosensors*, 12 (2022) 314.

22. R. Zhang, W. Zhang, Q. Yang, J. Dong, L. Ma, Z. Jiang and Y. Huang, *Journal of Energy Chemistry*, (2022) 1.
23. M. Yang, C. Li, Y. Zhang, D. Jia, R. Li, Y. Hou and H. Cao, *The International Journal of Advanced Manufacturing Technology*, 102 (2019) 2617.
24. X. Zhu, X. Zhang, L. Huang, Y. Liu, H. Zhang and S. Dong, *Chemical Communications*, 55 (2019) 9995.
25. Z. Huang, P. Luo, H. Zheng and Z. Lyu, *Journal of Alloys and Compounds*, 908 (2022) 164599.
26. X. Xiao, B. Mu, G. Cao, Y. Yang and M. Wang, *Journal of Science: Advanced Materials and Devices*, 7 (2022) 100430.
27. W. Qiao, Z. Li, W. Liu and E. Liu, *International Journal of Energy Research*, 46 (2022) 1766.
28. L. Cao, L. Kou, J. Li, J. Huang, J. Yang and Y. Wang, *Journal of Materials Science*, 53 (2018) 10270.
29. L. Liu, X. Meng, Z. Miao and S. Zhou, *Case Studies in Thermal Engineering*, 31 (2022) 101836.
30. L. Nan, C. Yalan, L. Jixiang, O. Dujuan, D. Wenhui, J. Rouhi and M. Mustapha, *RSC Advances*, 10 (2020) 27923.
31. T. Gao, Y. Zhang, C. Li, Y. Wang, Y. Chen, Q. An, S. Zhang, H. Li, H. Cao and H. Ali, *Frontiers of Mechanical Engineering*, 2022 (2022) 1.
32. H. Karimi-Maleh, H. Beitollahi, P.S. Kumar, S. Tajik, P.M. Jahani, F. Karimi, C. Karaman, Y. Vasseghian, M. Baghayeri and J. Rouhi, *Food and Chemical Toxicology*, (2022) 112961.
33. S.K. Bhatia, R.K. Bhatia, J.-M. Jeon, A. Pugazhendhi, M.K. Awasthi, D. Kumar, G. Kumar, J.-J. Yoon and Y.-H. Yang, *Fuel*, 285 (2021) 119117.
34. J. Sternberg, O. Sequerth and S. Pilla, *Progress in Polymer Science*, 113 (2021) 101344.
35. L.J. Tan, W. Zhu and K. Zhou, *Advanced Functional Materials*, 30 (2020) 2003062.
36. M. Saleem, M. Naz, B. Shoukat, S. Shukrullah and Z. Hussain, *Materials Today: Proceedings*, 47 (2021) S74.
37. L. Wang, Y. Wang, M. Wu, Z. Wei, C. Cui, M. Mao, J. Zhang, X. Han, Q. Liu and J. Ma, *Small*, 14 (2018) 1800737.
38. X. Zhang, C. Li, Y. Zhang, Y. Wang, B. Li, M. Yang, S. Guo, G. Liu and N. Zhang, *Precision Engineering*, 47 (2017) 532.
39. N. Yang, Z.-X. Luo, S.-C. Chen, G. Wu and Y.-Z. Wang, *ACS Applied Materials & Interfaces*, 12 (2020) 18952.
40. J. Tuo, Y. Zhu, L. Cheng, Y. Li, X. Yang, J. Shen and C. Li, *ChemSusChem*, 12 (2019) 2644.
41. H.W. Kim, H. Park, J.S. Roh, J.E. Shin, T.H. Lee, L. Zhang, Y.H. Cho, H.W. Yoon, V.J. Bukas and J. Guo, *Chemistry of Materials*, 31 (2019) 3967.
42. T. Liu, L. Zhang, W. You and J. Yu, *Small*, 14 (2018) 1702407.
43. J. Chen, H. Wang, J. Deng, C. Xu and Y. Wang, *Journal of Materials Chemistry A*, 6 (2018) 8986.
44. K. Ishimaru, T. Hata, P. Bronsveld, T. Nishizawa and Y. Imamura, *Journal of wood science*, 53 (2007) 442.
45. A. Osikoya, D. Wankasi, R. Vala, C. Dikio, A. Afolabi, N. Ayawei and E. Dikio, *Digest Journal of Nanomaterials and Biostructures*, 10 (2015) 125.
46. W. Qiao, W. Liu and E. Liu, *Energy*, 235 (2021) 121216.
47. S. Isikli, M. Lecea, M. Ribagorda, M.C. Carreño and R. Díaz, *Carbon*, 66 (2014) 654.
48. H. Karimi-Maleh, C. Karaman, O. Karaman, F. Karimi, Y. Vasseghian, L. Fu, M. Baghayeri, J. Rouhi, P. Senthil Kumar and P.-L. Show, *Journal of Nanostructure in Chemistry*, (2022) 1.
49. L. Zhao, L.Z. Fan, M.Q. Zhou, H. Guan, S. Qiao, M. Antonietti and M.M. Titirici, *Advanced materials*, 22 (2010) 5202.
50. W. Wang, Q. Hao, W. Lei, X. Xia and X. Wang, *Journal of Power Sources*, 269 (2014) 250.

51. H. Liu, H. Song, X. Chen, S. Zhang, J. Zhou and Z. Ma, *Journal of Power Sources*, 285 (2015) 303.
52. H. Xu, X. Li and G. Wang, *Journal of Power Sources*, 294 (2015) 16.
53. A. Ilnicka, M. Skorupska, M. Szkoda, Z. Zarach, P. Kamedulski, W. Zielinski and J.P. Lukaszewicz, *Scientific Reports*, 11 (2021) 1.
54. H. Karimi-Maleh, R. Darabi, M. Shabani-Nooshabadi, M. Baghayeri, F. Karimi, J. Rouhi, M. Alizadeh, O. Karaman, Y. Vasseghian and C. Karaman, *Food and Chemical Toxicology*, 162 (2022) 112907.
55. K. Guo, Y. Ma, H. Li and T. Zhai, *Small*, 12 (2016) 1024.
56. Y. Liu, Q. Sui, Y. Zou, C. Xiang, F. Xu, J. Xie and L. Sun, *International Journal of Electrochemical Science* 14 (2019) 5096.
57. Z. Fan, J. Yan, T. Wei, L. Zhi, G. Ning, T. Li and F. Wei, *Advanced Functional Materials*, 21 (2011) 2366.
58. W. Xiong, J.H. Kang, J.K. Kang and Y. Jung, *international Journal of Electrochemical Science*, 12 (2017) 8973.
59. L.L. Zhang, X. Zhao, H. Ji, M.D. Stoller, L. Lai, S. Murali, S. McDonnell, B. Cleveger, R.M. Wallace and R.S. Ruoff, *Energy & Environmental Science*, 5 (2012) 9618.
60. W. Qiao, Y. Wang, J. Zhang, W. Tian, Y. Tian and Q. Yang, *Journal of Environmental Management*, 289 (2021) 112438.
61. J. Jiang, H. Chen, Z. Wang, L. Bao, Y. Qiang, S. Guan and J. Chen, *Journal of colloid and interface science*, 452 (2015) 54.
62. D. Gueon and J.H. Moon, *ACS applied materials & interfaces*, 7 (2015) 20083.
63. M. Liu, C. Li, Y. Zhang, Q. An, M. Yang, T. Gao, C. Mao, B. Liu, H. Cao and X. Xu, *Frontiers of Mechanical Engineering*, 16 (2021) 649.
64. L. Sun, C. Tian, Y. Fu, Y. Yang, J. Yin, L. Wang and H. Fu, *Chemistry—A European Journal*, 20 (2014) 564.
65. C.P. Sugumaran, *Ionics*, 26 (2020) 1465.
66. Y. Li, R.-Q. Ren and X.-J. Jin, *International Journal of Electrochemical Science*, 11 (2016) 9599.
67. T. Gao, Y. Zhang, C. Li, Y. Wang, Q. An, B. Liu, Z. Said and S. Sharma, *Scientific reports*, 11 (2021) 1.
68. H. Maleh, M. Alizadeh, F. Karimi, M. Baghayeri, L. Fu, J. Rouhi, C. Karaman, O. Karaman and R. Boukherroub, *Chemosphere*, (2021) 132928.
69. L.-F. Chen, X.-D. Zhang, H.-W. Liang, M. Kong, Q.-F. Guan, P. Chen, Z.-Y. Wu and S.-H. Yu, *ACS nano*, 6 (2012) 7092.
70. M. Yang, C. Li, Z. Said, Y. Zhang, R. Li, S. Debnath, H.M. Ali, T. Gao and Y. Long, *Journal of Manufacturing Processes*, 71 (2021) 501.
71. F.M. Hassan, V. Chabot, J. Li, B.K. Kim, L. Ricardez-Sandoval and A. Yu, *Journal of Materials Chemistry A*, 1 (2013) 2904.
72. E. Frackowiak, G. Lota, J. Machnikowski, C. Vix-Guterl and F. Béguin, *Electrochimica Acta*, 51 (2006) 2209.
73. G.P. Pandey, T. Liu, C. Hancock, Y. Li, X.S. Sun and J. Li, *Journal of Power Sources*, 328 (2016) 510.
74. Q. Zhang, Z. Liu, B. Zhao, Y. Cheng, L. Zhang, H.-H. Wu, M.-S. Wang, S. Dai, K. Zhang and D. Ding, *Energy Storage Materials*, 16 (2019) 632.
75. S. Hui, Z. Ying, X. Lin, J. Sun, Y. Wang, Q. Fu and J. Li, *Journal of Alloys and Compounds*, 846 (2020) 156235.
76. Y. Cheng, L. Huang, X. Xiao, B. Yao, L. Yuan, T. Li, Z. Hu, B. Wang, J. Wan and J. Zhou, *Nano energy*, 15 (2015) 66.
77. H. Guo and Q. Gao, *Journal of Power Sources*, 186 (2009) 551.

78. H. Chen, D. Liu, Z. Shen, B. Bao, S. Zhao and L. Wu, *Electrochimica acta*, 180 (2015) 241.
79. Y. Liu, J. Zhou, L. Chen, P. Zhang, W. Fu, H. Zhao, Y. Ma, X. Pan, Z. Zhang and W. Han, *ACS applied materials & interfaces*, 7 (2015) 23515.
80. T. Gao, C. Li, Y. Wang, X. Liu, Q. An, H.N. Li, Y. Zhang, H. Cao, B. Liu and D. Wang, *Composite Structures*, 286 (2022) 115232.

© 2022 The Authors. Published by ESG (www.electrochemsci.org). This article is an open access article distributed under the terms and conditions of the Creative Commons Attribution license (<http://creativecommons.org/licenses/by/4.0/>).